Atmospheric mercury in the Southern Hemisphere – Part 2: Source apportionment analysis at Cape Point station, South Africa.

Johannes Bieser[1], Hélène Angot[2], Franz Slemr[31], Lynwill Martin[4]

Corresponding authors: johannes.bieser@hzg.de Lynwill.Martin@weathersa.co.za

[1]Helmholtz-Zentrum Geesthacht (HZG), Institute of Coastal Research, Max-Planck-Str. 1, D-21502 Geesthacht, Germany

[2]Institute of Arctic and Alpine Research, University of Colorado Boulder, Boulder, CO, USA.

[3]Max-Planck-Institut für Chemie (MPI), Air Chemistry Division, Hahn-Meitner-Weg 1, D-55128 Mainz, Germany

[4]South African Weather Service c/o CSIR, P.O.Box 320, Stellenbosch 7599, South Africa

Abstract

Mercury (Hg) contamination is ubiquitous. In order to assess its emissions, transport, atmospheric reactivity, and deposition pathways, worldwide Hg monitoring has been implemented over the past 10-20 years, albeit with only few stations in the southern hemisphere. Consequently, little is known about the relative contribution of marine and terrestrial Hg sources, which is important in the context of growing interest in effectiveness evaluation of Hg mitigation policies. This paper constitutes Part 2 of the study describing a decade of atmospheric Hg concentrations at Cape Point, South Africa, i.e. the first long-term (> 10 years) observations in the Southern Hemisphere. Building on the trend analysis reported in Part 1, here we combine atmospheric Hg data with a trajectory model to investigate sources and sinks of Hg at Cape Point. We find that the continent is the major sink and the ocean, especially its warm regions (i.e. the Agulhas Current), is the major source for Hg.
Further, we find that mercury concentrations and trends from long range transport are independent of the source region (e.g. South America, Antarctica) and thus indistinguishable. Therefore, by filtering out air masses from source and sink regions we are able to create a dataset representing a southern hemispheric background Hg concentrations. Based on this dataset we were able to show that the inter-annual variability of Hg concentrations at Cape Point is not driven by climatology and changes in atmospheric circulation but rather due to changes in global emissions (gold mining and biomass burning).

1. Introduction

Mercury (Hg) is a toxic pollutant that is ubiquitous in the environment. Due to anthropogenic emissions, the amount of mercury in the atmosphere has increased sevenfold since pre-industrial times (Amos et al., 2013). Mercury occurs in the atmosphere as gaseous oxidized mercury (GOM), particle bond mercury (PBM) and predominantly (~95%) as gaseous elemental mercury (GEM). Because of its atmospheric lifetime of about 1 year, once emitted into the atmosphere, GEM is transported on hemispheric and global scales (Slemr et al., 2018). Since 2017 usage and emissions of Hg are regulated under the UN Minamata Convention on Mercury (UNEP, 2013). This UN convention commits its member states to assess the current state of mercury pollution, take actions to reduce mercury emissions, and to evaluate the success of these measures on a regular basis.

In order to assess the impact of emission reductions on the system it is necessary to better understand the sources and sinks driving atmospheric mercury cycling. Especially in the southern hemisphere there has been a lack of long-term atmospheric observations that allow to investigate and distinguish long-term trends from the natural variability of atmospheric Hg concentrations. So far, the only long-term observations in the southern hemisphere with measurements over more than 10 years have been and are performed at Cape Point (CPT), South Africa, where GEM has been measured since 1995 (Baker et al., 2002, Slemr et al., 2008). At CPT, for the first ten years (September 1995 to December 2004) GEM concentrations showed a decreasing trend (Slemr et al., 2008, Martin et al., 2017) while Martin et al. (2017) identified an increasing trend for the last ten years (March 2007 to June 2015). Yet the reason for the observed trends is unclear and there was no explanation for the change in sign from a decreasing to an increasing trend.

This work is presented in two accompanying papers where the first one (Slemr et al., 2020) focuses on long-term trends in the southern hemisphere over the last ten years based on measurements at CPT and Amsterdam Island (AMS) which is operational since 2012. The key finding of that paper is that since 2007 GEM concentrations at CPT seem to have been increasing while no significant trend was found in the 2012 – 2017 period both at CPT and AMS. The upward CPT trend in 2007 – 2017 period seems to be driven by exceptionally low Hg concentrations in 2009 and above average concentrations in 2014.

Here, we combine ten years of GEM (2007 – 2016) observations at CPT with calculated hourly backward trajectories in order to investigate sources and sinks for mercury and to quantify the impact of long-term changes in atmospheric circulation patterns on observed GEM concentrations at CPT. The aim of this study is to:

- distinguish between local changes at CPT and hemispheric GEM trends;
- identify source and sink regions for GEM at CPT;
- estimate the natural variability of GEM concentrations at CPT in order to distinguish them from other effects such as changing emissions.

This paper aims to improve our understanding of mercury cycling in the southern hemisphere. For this, we elaborate on the research question whether concentrations and trends observed at CPT are dominated by local signals or representative for mercury cycling across large parts of the southern hemisphere. Based on backward trajectories and statistical modeling we investigate source and sink regions for mercury observed at Cape Point and the impact of inter-annual variability on atmospheric transport patterns and emissions processes.

2. Methodology

2.1 Observations

This study is based on ten years (2007-2016) of continuous GEM measurements at Cape Point (CPT, 34º21′S, 18º29′E), South Africa. The CPT measurement site is part of the GAW (Global Atmospheric Watch) baseline monitoring observatories of the World Meteorological Organization (WMO). It is located at the southernmost tip of the Cape Peninsula on top of the cliff at an altitude of 230 m (a.s.l.). There are no major local Hg sources and the nearest city, Cape Town, is located 60 km to the north (see Fig. 1). The station has been in operation since the 1970ties and, besides GEM, several other pollutants are measured on a regular basis. These include CO_2, CO, ozone, methane, and radon (^{222}Rn) which we use to substantiate the findings on mercury. A detailed description of the CPT station can be found in the accompanying paper (Slemr et al., 2020).

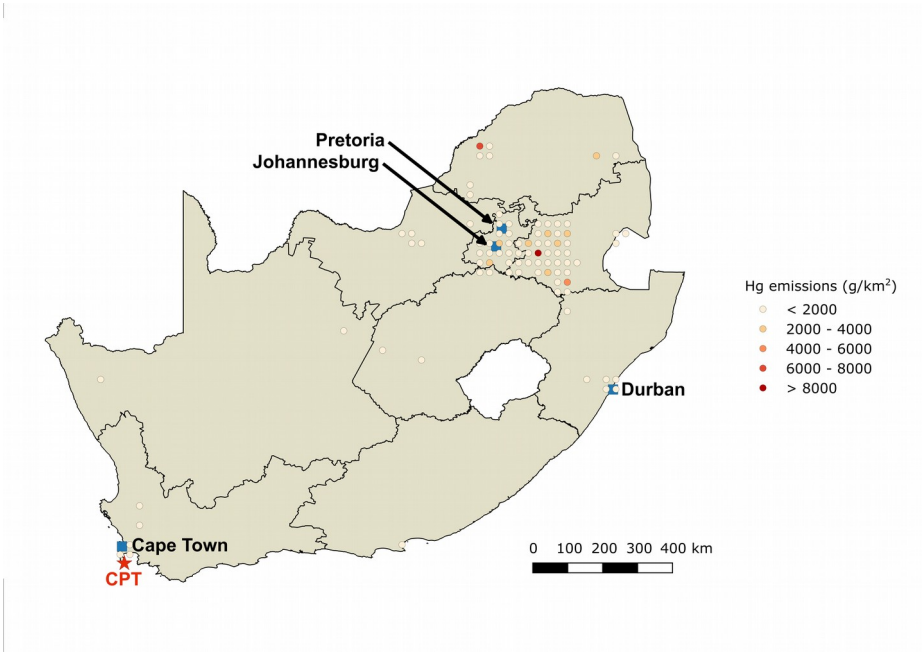

Figure 1: Location of the Cape Point site (CPT, red star), at the southernmost tip of the Cape Peninsula, and of known anthropogenic mercury emission sources (in g/km², Global Mercury Assessment 2018 emission inventory (Frits Steenhuisen, personal communication, July 2017)) in South Africa. This map was made with QGIS.

2.2 Modeling

GEM measurements at CPT are performed continuously with a 15 min sampling interval. The GEM measurements were aggregated to hourly averages and for each hourly measurement an ensemble of 5-day backward trajectories was calculated using the Hybrid Single Particle Lagrangian Trajectory Model (HYSPLIT) (Stein et al., 2015) (Fig. 2). For the hourly trajectory ensembles we used different starting altitudes in order to capture the model uncertainty due to the model's initial conditions. The HYSPLIT model was run for ten years (2007 to 2016) using GDAS (Global Data Assimilation System) 0.5°x0.5° degree meteorological inputs based on the NCEP/NCAR reanalysis dataset (Kalnay et al., 1996, NOAA, 2004).

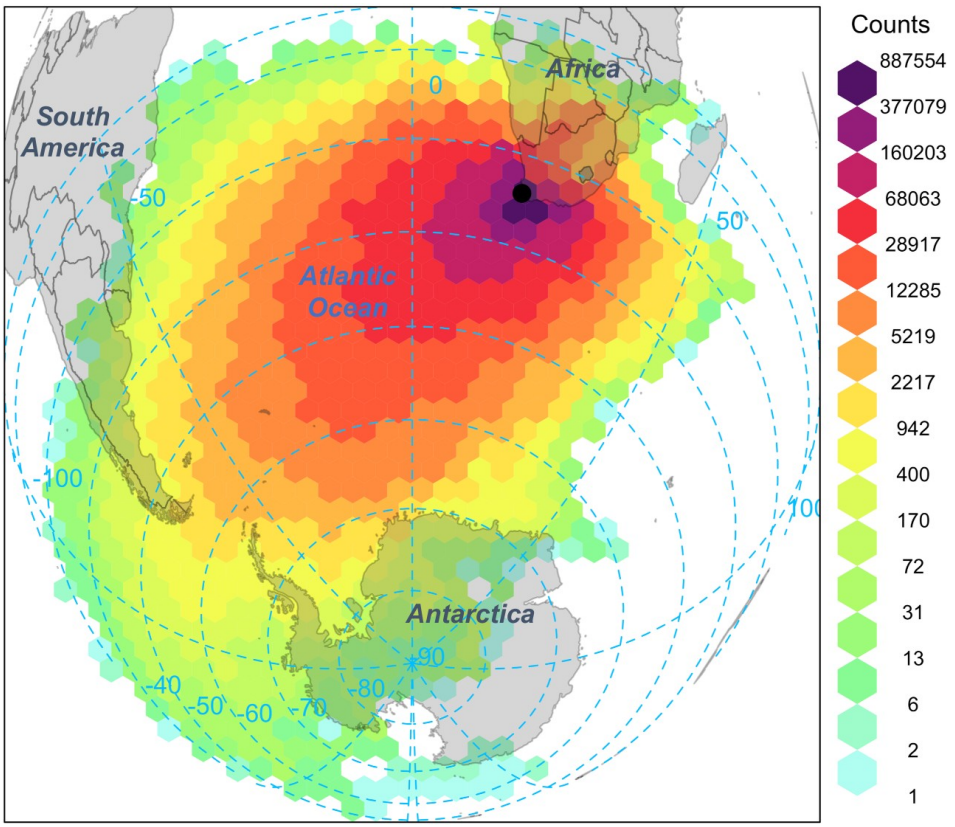

Fig. 2: Origin of air masses influencing the Cape Point site (black dot). Gridded back trajectory frequencies using an orthogonal map projection with hexagonal binning. The tiles represent the number of incidences. 2007-2016 hourly back trajectories were computed using the HYSPLIT model (Stein et al. 2015) and the figure was made using the R package openair (Carslaw and Ropkins, 2012).

2.3 RegionalizationThe trajectories were categorized into six source regions depending on their travel path (Figure 3, Table 1). These categories are:

- **Local**

  Air parcels which traveled less than 100 km absolute distance to CPT over the last four days are considered to be local air masses.

- **Continental**

  Air parcels that spend more than 80% of travel time over the African continent during the last four days.

- **Eastern Ocean**

  Air parcels which did not travel over land and did not go west of 30° E within the last four days.

- **South American**

  Air parcels which were west of 30°W within the last four days.

- **Antarctic**

  Air parcels which were south of 55° S within the last four days.

- **Atlantic**

  Air masses which do not fall within the other categories and spend more than 80% of the time over the Atlantic Ocean. This category makes up the majority of all trajectories.

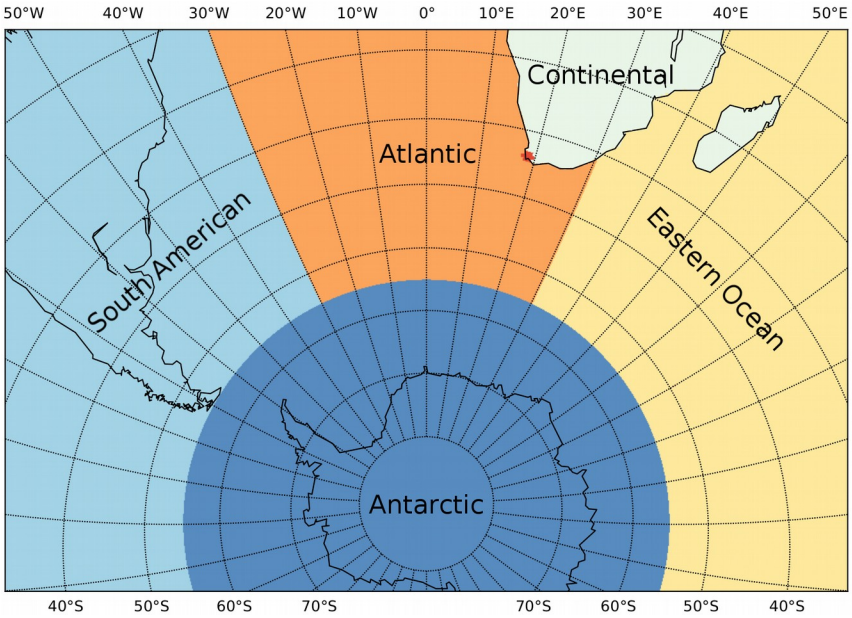

Figure 3: Depiction of the regionalization used for this study: Local (red), Continental (light green), Eastern Ocean (yellow), South American (turquoise), Antarctic (blue), Atlantic (orange),

The categorization of air parcels depends on the definition of regions of origin and the travel time chosen for the algorithm. We calculated 5-day backward trajectories and experimented with different cutoff values to determine the source regions of the air masses (Table 1). For this study we chose a cutoff time of 4 days to determine long range transport from Antarctica and South America. However, the choice of cuttoff times of 3 or 5 days did not change the conclusions of our study. This decision is based on tests with different cutoff times and on the fact that the uncertainty of the trajectories grows with travel time (Engström and Magnusson, 2009). Moreover, air parcels are often a mixture of different source regions (e.g. Atlantic/continental). As an additional test for the calculated categorization we used secondary parameters such as ^{222}Rn, CO, CO_2, CH_4, and O_3. ^{222}Rn is a radioactive gas of predominantly terrestrial origin with a half-life of 3.8 days. Thus, high ^{222}Rn concentrations mark air masses which recently passed over the continent such as “Continental” and “Local”. Other examples are the distinction of long-range transport from South America from Atlantic air masses. Here, we would also expect higher concentrations of other anthropogenic pollutants (e.g. CO_2, CH_4).

Days	Antarctic	S. America	Continental	Eastern O.	Atlantic	Local
2	1778 (1%)	150 (< 1%)	14580 (9%)	5930 (4%)	143478 (86%)	1760 (1%)
3	11800 (7%)	3614 (2%)	10596 (6%)	7842 (5%)	132876 (79%)	926 (1%)
4	26696 (16%)	12756 (8%)	7928 (5%)	7882 (5%)	111770 (67%)	550 (<1%)
5	39710 (24%)	22960 (14%)	5906 (4%)	6876 (4%)	91666 (55%)	370 (<1%)

Table 1: Impact of travel time cutoff on air parcels source region categorization. Total and relative allocation of trajectories to each source region depending on air parcel travel time.

2.4 Identification of source/sink regions

In order to evaluate source and sink regions we calculated the 10th and 90th percentile of GEM measurements for each season (seasons being defined as three-month intervals: DJF (summer), MAM (autumn), JJA (winter), SON (spring)). This seasonal filter proved to be necessary to remove the annual cycle in GEM concentrations driven (among others) by the seasonality of emissions, planetary boundary layer height, and transport patterns. Furthermore, we filtered out mercury depletion events, of unknown origin (Brunke et al. 2010), which were defined as hourly average GEM concentrations of less 0.25 ng/m³.

For the source/sink region analysis we interpolated hourly trajectory locations onto a polar stereographic grid centered over the South Pole and calculated the total amount of trajectories traveling through each grid cell over the ten-year (2007-2016) period. We then performed the same procedure for the trajectories of the 10th and 90th percentile GEM concentrations. By dividing these percentile maps by the total amount of trajectories traveling through each grid cell, we created maps indicating the regional prevalence of high and low GEM concentrations.

In the theoretical case of perfectly homogeneous, evenly distributed sources and sinks each grid cell would have a value of 0.1 indicating that 10% of all air parcels in each grid cell belong to the 10% highest/lowest GEM observations. Deviations from this uniform distribution are then interpreted as source/sink regions for high/low GEM concentrations. E.g. a value of 0.2 indicates that twice as many high/low GEM concentrations originate from a given grid cell compared to a uniform distribution.

To better distinguish the 10th and 90th percentile plots we chose opposite color schemes for the 10th and 90th percentile plots. In the case of the 90th percentile plots red color indicates source regions for high GEM concentrations (i.e. > 0.1) while blue color indicates the absence of sources in this region (Fig 4a). For the 10th percentile plots blue color indicates sink regions for GEM concentrations (Fig 4b) while red color indicates the absence of sinks. It is important to note that an absence of sources is not equal to the presence of sinks and vice versa. Figure 4 gives an example of these plots for air masses attributed to the 'Atlantic' category for ^{222}Rn measurements. This plot serves as an evaluation of the regionalization algorithm. It can be seen that high ^{222}Rn concentrations are found only in air masses that traveled over the continent (Fig 4a). Similarly, Figure 4b depicts the fact that no measurements with low ^{222}Rn concentrations were found in air masses that traveled along the coast line, indicating an impact of terrestrial sources. Finally, this procedure is sensitive to the total amount of trajectories traveling through a grid cell which leads to low signal to noise ratios in the outskirts of the plot where only few trajectories originate at all. We used a cutoff value of 10 hits and discarded all grid cells with fewer hits but this still leads to a few non-significant hot spots at the outskirts of the domain (e.g. Fig 4a in Antarctica).

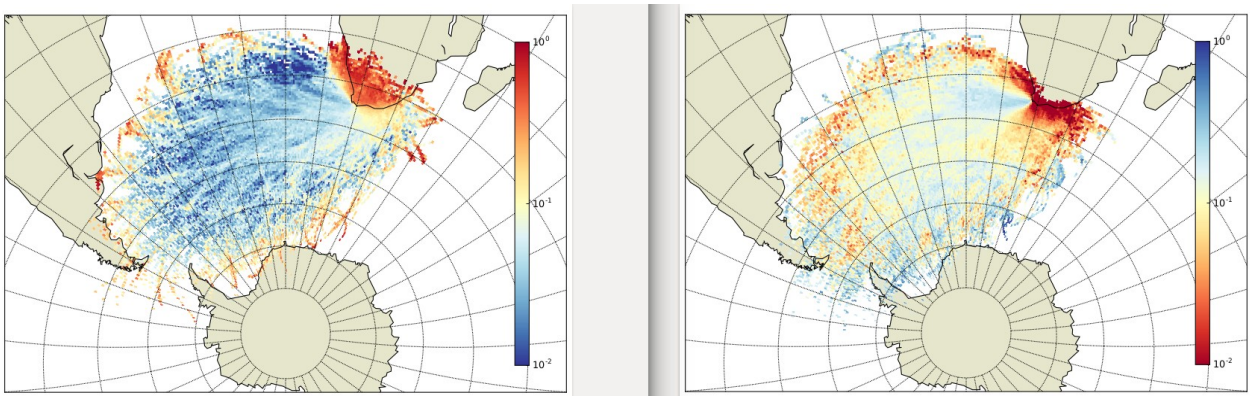

Figure 4: Distribution map for the 90th percentile highest ^{222}Rn concentrations (left) and the 10th percentile lowest ^{222}Rn concentrations (right) measured at Cape Point. Values are the dimensionless prevalence of air parcels of a given concentration percentile ranging from 0 to 1. This means that a homogeneous distribution of source and sink regions would lead to a plot with values of 0.1 everywhere. Deviations from this value indicate source and sink regions. See also the description in Section 2.4.

3. Results and Discussion

In this section we use backward trajectories of the 10th and 90th percentile GEM concentrations observed at Cape Point to identify the major source and sink regions for mercury *(Section 3.1 "Source and sink regions")*. We find that the eastern ocean with the warm Agulhas current is the major source region and the continent is the major sink region. We then compare the regional patterns of GEM with other pollutants *(Section 3.2 "Comparison of regionalized data")* and find that GEM shows a distinct pattern compared to pollutants of terrestrial, anthropogenic and photochemical origin. In Section 3.3 *"Regional trends"* we investigate distinct mercury trends for each region. We find that air masses from long range transport (South America, Antarctica) show no distinct trends which indicates that they are representative of the SH background. In Section 3.4 *"Regional abundance"* we investigate what impact changing atmospheric circulation may have on the GEM trend observed at Cape Point and found it to be negligible. Instead we find, that the annual average GEM concentrations depend on the regions with highest (estern ocean) and lowest (continental) GEM concentrations in air masses. Finally, in Section 3.5 *"Inter-annual variability"* we try to explain the inter-annual variability of GEM concentrations observed at Cape Point with changes in global emissions. We show that biomass burning and gold mining emissions can partly explain years with exceptionally high (2014) or low (2009) GEM concentrations.

3.1 Source and sink regions

Figure 5 shows the 10th and 90th percentile maps for all GEM measurements over the whole period 2007-2016 (Fig. 5). It can be seen that low GEM concentrations originate almost exclusively from air masses which traveled over the continent (Fig 5b). This result is in line with a cluster analysis performed by Venter et al. (2015) *"Air masses that had passed over the very sparsely populated semi-arid Karoo region, almost directly to the north of CPT GAW, were mostly associated with [...] lower GEM values"*. It is also consistent with the finding of Slemr et al. (2013) that southern Africa, based on GEM vs ^{222}Rn correlations, is a net sink region. The reason for this is probably a mixture of near zero emissions in the region and dry deposition onto the surface.

Over the Atlantic Ocean, low GEM concentrations are in line with a uniform distribution with values mostly only slightly below the equilibrium value of 0.1. The exception are air masses that travelled over the ocean east of Cape Point where almost no low concentration GEM measurements originated. Looking at the highest 90th percentile of GEM concentrations, air masses travelling over the ocean show a lower abundance with the exception of a patch east of Cape Point (Fig 5a).

The picture becomes clearer when plotting trajectories independently for each of the previously defined regions (Fig. 6). It can be seen that the eastern ocean sector is the predominant source region of air masses with elevated GEM concentrations (Fig. 6e). In this region the Agulhas Current transports warm water from the Indian Ocean to the Atlantic Ocean and we

identify this warm current as a major mercury source in the region. For continental air masses (Fig. 6b), certain source regions can be identified. These coincide with known major Hg emitters, mainly coal combustion for energy production (Fig. 1). For air masses representing long range transport (Atlantic, South American, Antarctic) frequency values of the 90th percentile highest GEM concentrations are mostly around 10% indicating no specific sources or sinks in these regions.

19

20

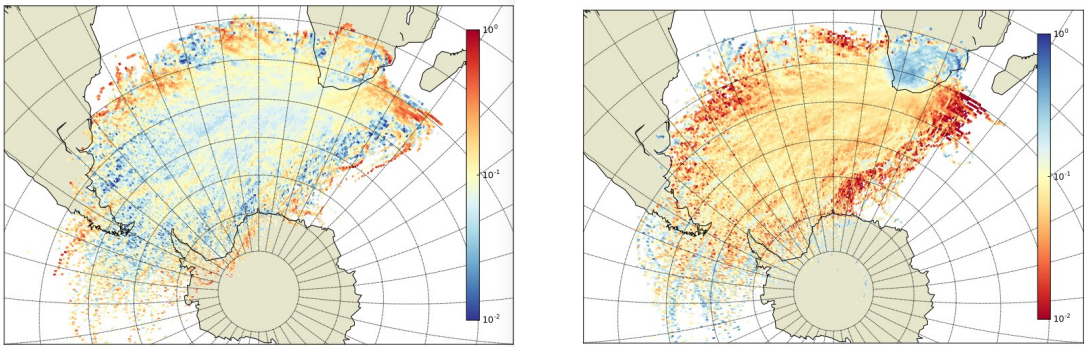

*F*igure 5: Prevalence of highest (90th percentile) (left) and lowest (10th percentile) (right) GEM concentrations u*sing all hourly trajectories over ten years.*

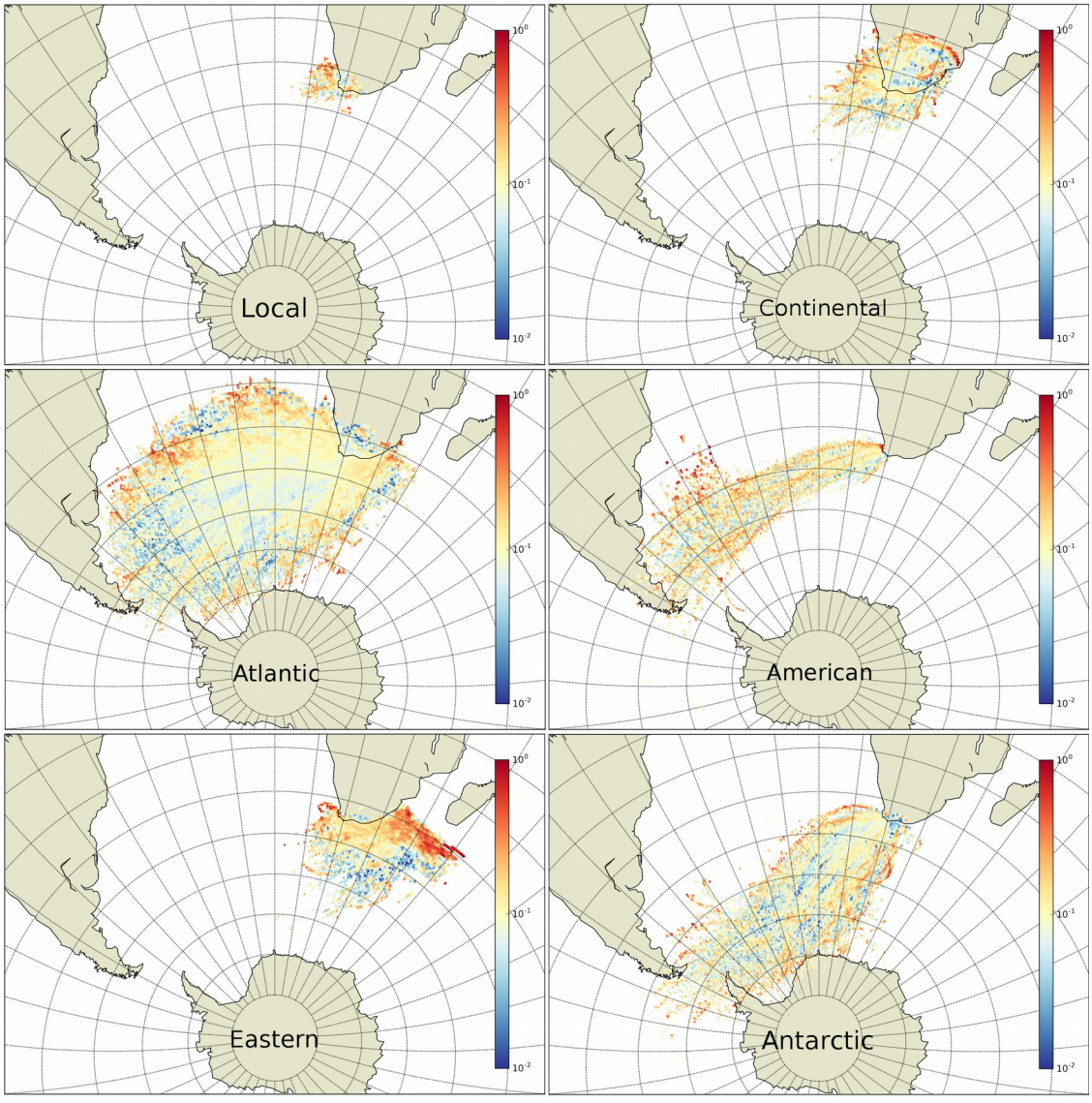

Figure 6: 90th percentile highest GEM concentrations for air masses from six source regions. Red color means source regions, blue one absence of emissions in that region.

Looking at the 10th percentile of lowest GEM concentrations, regional and continental air masses can be identified as the single most important sink region (Fig. 7a,b). There are also some continental areas with a high prevalence of low Hg concentrations attributed to the Atlantic sector. These can be interpreted as air parcels with a mixed continental/Atlantic travel path that have been attributed as Atlantic air masses by the algorithm as they did not spend enough time over the continent to be attributed to this sector. Finally, there are no air masses with low GEM concentrations originating from the eastern ocean sector (Fig. 7e).

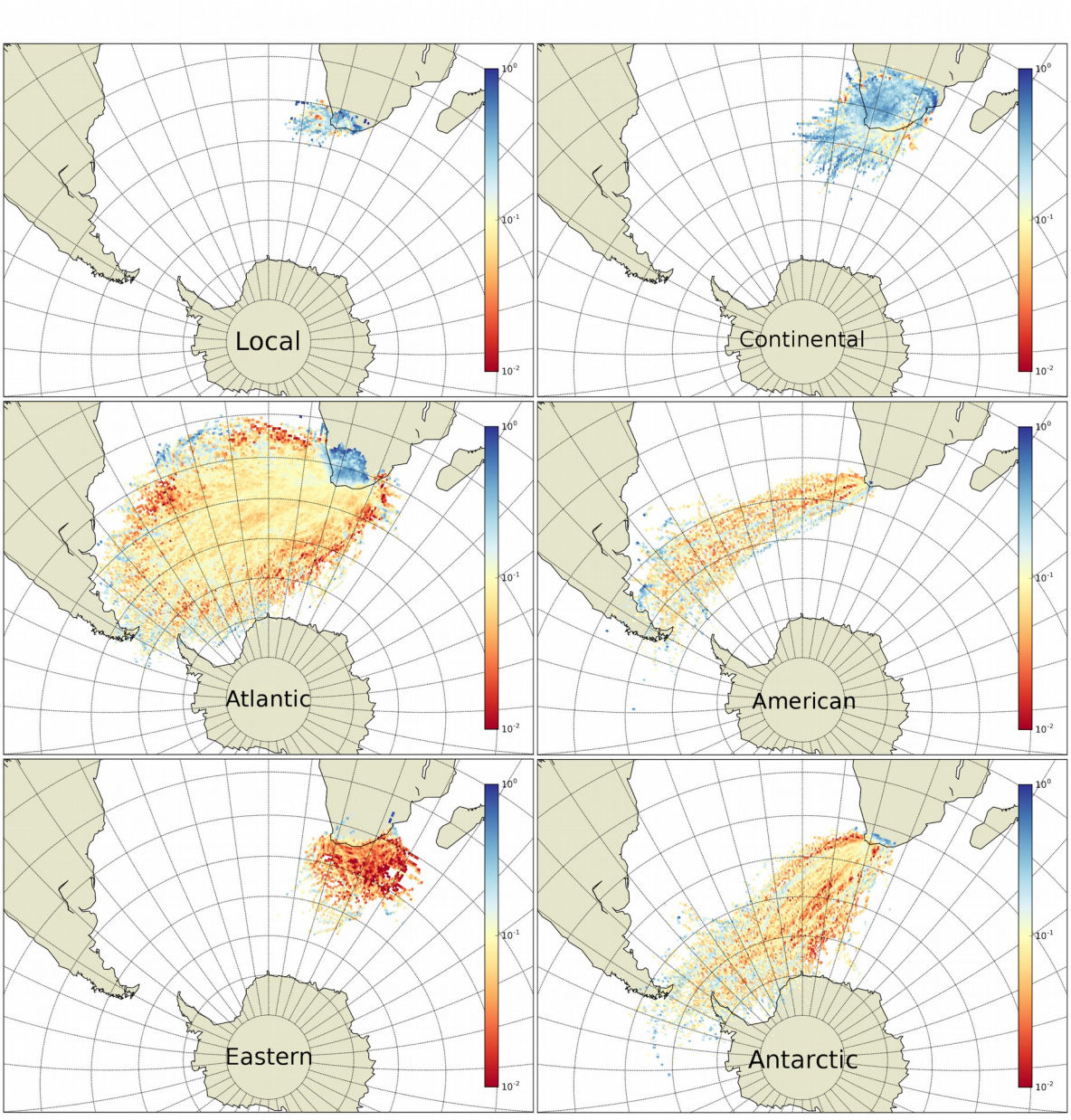

Fig. 7: 10th percentile lowest Hg concentrations for six source regions. Blue colors indicate sink regions, red color absence of sinks. Low values are almost exclusively linked to continental and local air masses.

To further investigate the processes behind the observed source and sink regions, we regard seasonal trajectory maps (Fig. 8). This analysis reveals, that the high GEM concentrations associated to air masses from the eastern ocean occur mainly during austral spring and summer. This is consistent with the seasonal variation of GEM concentrations at Cape Point shown in Figure 2 of the companion paper (Slemr et al., 2020). Temperature or primary production and a related increase in evasion of GEM (with a large impact of reemissions of legacy Hg) from the ocean are thus the likely reason for these observations.

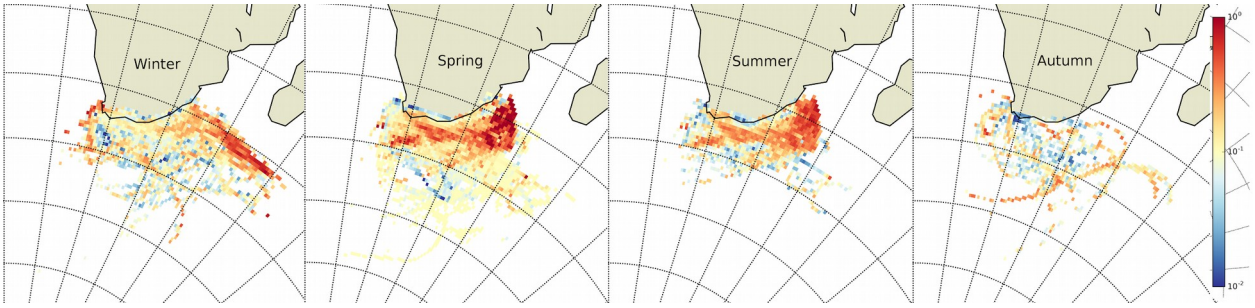

Figure 8: Seasonal breakdown of 90th percentile highest Hg concentrations from the eastern ocean source region. Highest Hg concentrations are mostly associated to Austral spring and summer which supports primary production as a potential source for oceanic Hg releases.

3.2 Comparison of regionalized data

Annual and monthly averages and medians for each source region of 4-days backward trajectory were calculated for GEM, CO_2, ^{222}Rn, CO, CH_4, and O_3. Here we compare the annual medians for all species and discuss the implications this comparison provides on regionalization.

Year	Antarctic	South America	Continental	Eastern Ocean	Atlantic	Local
	Annual median GEM concentration in ng m^{-3}, number of measurements					
2007	0.975, 2406	0.968, 1388	1.003, 412	1.046, 378	0.983, 6946	0.982, 39
2008	0.976, 1939	0.994, 811	0.992, 550	1.047, 453	1.002, 7903	0.883, 10
2009	0.910, 2457	0.904, 944	0.904, 950	0.933, 544	0.908, 9482	1.025, 27
2010	0.995, 2237	0.982, 1010	0.929, 918	1.036, 706	0.996, 10438	1.084, 18
2011	0.984, 1874	0.952, 941	0.978, 890	1.006, 1282	0.979, 8851	0.964, 69
2012	1.074, 2576	1.077, 1436	1.035, 453	1.063, 541	1.068, 10012	1.030, 62
2013	1.048, 2523	1.057, 1260	0.911, 555	1.069, 191	1.029, 8069	0.938, 48
2014	1.057, 2309	1.079, 947	1.045, 943	1.206, 929	1.098, 10791	1.090, 92
2015	1.009, 2330	1.009, 1020	0.992, 546	0.987, 482	0.998, 11486	1.017, 46
2015	1.030, 2206	1.024, 990	0.986, 612	1.055, 740	1.015, 9935	0.934, 72
average	**1.006**	**1.005**	**0.998**	**1.045**	**1.008**	**0.995**

Table 2: Annual median GEM concentrations.

Table 2 shows the annual median GM concentrations. The highest annual median GEM concentrations were found for “Eastern Ocean” in 6 of 10 years. The lowest annual GEM concentrations were almost always either of “Local” or “Continental” origin. Annual median

GEM concentrations for “South American”, “Antarctic” and “Atlantic” lie close to each other and are in the middle in varying order. Annual average GEM concentrations behave similarly (not shown).

Year	Antarctic	South America	Continental	Eastern Ocean	Atlantic	Local
	Annual median ^{222}Rn concentration in mBq m^{-3}, number of measurements					
2007	294, 2770	265, 1584	804, 432	685, 376	350, 8758	842, 38
2008	241, 1492	283, 604	2120, 502	345, 412	349, 6940	
2009	230, 1982	275, 840	1623, 912	436, 548	345, 8306	1755, 26
2010	257, 1942	315, 780	2413, 784	449, 486	351, 9126	1326, 16
2011	208, 2546	288, 1086	2464, 1104	488, 1288	370, 10536	1612, 88
2012	184, 2658	231, 1510	1483, 548	413, 866	345, 10636	3273, 56
2013	252, 3104	174, 1650	2335, 630	489, 504	329, 10966	1709, 56
2014	249, 2296	255, 938	2195, 948	532, 968	337, 10928	1737, 74
2015	339, 2216	338, 1030	1786, 642	718, 564	348, 11510	803, 52
2015	244, 2346	209, 1296	2667, 626	530, 802	385, 10998	1656, 78
average	**250**	**263**	**1989**	**509**	**351**	**1635**

Table 3: Annual median ^{222}Rn concentrations.

Table 3 shows the annual median ^{222}Rn concentrations. The highest ^{222}Rn annual median concentrations were found for the regions “Continental” or “Local”, as expected for a radioactive trace gas of almost exclusively terrestrial origin and half-life of 3.8 days (Zahorowski et al., 2004). The lowest and second lowest ^{222}Rn concentrations were found in air masses attributed to “South American” or “Antarctic”. “Atlantic” median average concentrations are somewhat higher than “Antarctic” and “South American” but their interannual variation is the smallest of all. “Eastern Ocean” median concentrations are somewhat higher than the “Atlantic” ones which is likely due to proximity of African continent. The average concentrations behave similarly.

The regionalized median annual mixing ratios of CO, CO_2, CH_4, O_3 are shown in Supporting Information. Annual medians of CO, CO_2, and CH_4, all of predominantly terrestrial origin behave similarly to those of ^{222}Rn. Ozone, although not of terrestrial but of photochemical origin in NO_X rich environments, also fits this pattern because its mixing ratios are highest in “Local” or “Continental” air masses where the highest NO_X mixing ratios are expected. Annual averages behave similarly to annual medians.

In summary GEM, with highest concentrations in air masses attributed mostly to “Eastern Ocean” and the lowest ones found either in “Local” or “Continental”, shows a pattern opposite to all the other species mentioned above. Its different pattern clearly shows that its sources are predominantly oceanic and the sinks terrestrial. The results reported above apply for regionalization using 4-days backward trajectories. Regionalization with 3 or 5-days backward trajectories provides similar results. Moreover, GEM concentrations in the sectors Atlantic, South American, and Antarctic are so similar that we interpret these as the southern hemispheric background.

3.3 Regional trends

Table 4 shows the regionalized trends calculated from the monthly median concentrations or mixing ratios. Regionalised trends for GEM, CO_2, ^{222}Rn, CO, CH_4, and O_3 were calculated from regional monthly averages and medians using least square fit. Months with less than 10 measurements were not considered. This restriction applies mostly to region “Local” resulting in too few monthly values for trend calculation. The trends of ^{222}Rn and O_3 are insignificant for all regions. The trend differences are tested for significance by comparison of averages (Kaiser and Gottschalk, 1972) using the slope and its uncertainty as an average and its standard deviation, respectively.

Trace gas	Region	Slope	N, significance	Unit
GEM	Antarctic	10.84 ± 2.63 (a) 9.62 ± 2.69 (m)	112, >99.9%	pg m^{-3} yr^{-1}
	South American	10.16 ± 2.74 (a) 10.15 ± 2.80 (m)	111, >99.9%	
	Continental	8.40 ± 4.25 (a) 6.27 ± 4.02 (m)	91, ns	
	Eastern Ocean	5.20 ± 3.77 (a) 6.33 ± 3.80 (m)	67, ns	
	Atlantic	8.64 ± 2.59 (a) 8.13 ± 2.54 (m)	115, >99%	
CO_2	Antarctic	2.186 ± 0.023 (a) 2.196 ± 0.022 (m)	116, >99.9%	ppm yr^{-1}
	South American	2.171 ± 0.025 (a) 2.180 ± 0.022 (m)	116, >99.9%	
	Continental	2.246 ± 0.048 (a) 2.226 ± 0.044 (m)	90, >99.9%	
	Eastern Ocean	2.242 ± 0.049 (a) 2.210 ± 0.058 (m)	73, >99.9%	
	Atlantic	2.182 ± 0.023 (a) 2.196 ± 0.019 (m)	119, >99.9%	
CH_4	Antarctic	6.320 ± 0.484 (a) 6.776 ± 0.391 (m)	116, >99.9%	ppb yr-1
	South American	5.789 ± 0.528 (a) 6.712 ± 0.395 (m)	118, >99.9%	
	Continental	7.298 ± 0.708 (a) 6.732 ± 0.595 (m)	95, >99.9%	
	Eastern Ocean	7.225 ± 0.695 (a) 7.230 ± 0.610 (m)	76, >99.9%	
	Atlantic	6.670 ± 0.486 (a) 6.840 ± 0.388 (m)	119, >99.9%	
CO	Antarctic	-1.166 ± 0.385 (a) -0.527 ± 0.260 (m)	115, >99% (a) ns (m)	ppb yr^{-1}
	South American	-1.380 ± 0.397 (a) -0.731 ± 0.281 (m)	117, >99% (a) >95% (m)	
	Continental	-1.027 ± 0.823 (a) -1.055 ± 0.731 (m)	92, ns (a) ns (m)	
	Eastern Ocean	-0.010 ± 0.816 (a) -0.133 ± 0.781 (m)	75, ns (a) ns (m)	
	Atlantic	-1.007 ± 0.364 (a) -0.506 ± 0.271 (m)	119, >95% (a) ns (m)	

306 *Table 4: Trends of GEM, CO_2, CH_4, and CO calculated by least square fit from monthly averages (a) and*
307 *medians (m). Months with less than 10 measurements were not considered, which applies to most*
308 *"Local" months. Trends of ^{222}Rn and O_3 were insignificant for all regions.*

309 The trends of ^{222}Rn and O_3 are insignificant for all regions. CO_2 and CH_4 upward trends are
310 significant for all regions. The regional CO_2 trends for "Antarctic" and "Atlantic" are with 2.18 –
311 2.20 ppm yr^{-1} comparable. Comparable, although with 2.21 – 2.25 ppm yr^{-1} significantly higher,
312 are also the trends for "Continental" and "Eastern Ocean". The trend for "South American" is

the smallest of all. The CH_4 trends show the same pattern with the trend for “South American” being the smallest, too. The trends for “Antarctic” and “Atlantic” are comparable and somewhat higher. The highest and comparable are the trends for “Continental” and “Eastern Ocean”. The similar pattern for CO_2 and CH_4 trends is consistent with terrestrial sources of these trace gases. The trend for CO is always downward, although significant only for “South American” region when calculated both from monthly averages and medians.

Three source regions provide significant trends for GEM when calculated both from monthly averages and medians. The trends for “Antarctic” and “South American” air masses are comparable and significantly higher than the trend for the “Atlantic” region. This pattern is different from those of CO_2 and CH_4 with smaller trends for “South American” and higher ones for “Atlantic” and “Antarctic”. In summary, the patterns of GEM, CO_2, and CH_4 trend differences provide an additional piece of evidence for an oceanic GEM source and are consistent with the patterns of annual medians presented in section 3.2. The fact that GEM trends for the regions “Antarctic” and “South American” are almost identical indicates homogeneous behaviour of GEM in the southern hemisphere with no pronounced longitudinal gradient. We note that the overall trend of GEM concentrations is close to that for the “Atlantic” region to which two thirds of all GEM measurements are allocated.

3.4 Regional abundance

Air masses from long range transport (Atlantic, Antarctic, South American) make up 90% of all air masses observed at Cape Point. Seasonally averaged observed concentrations from these regions show a high correlation with the averages of all observations at Cape Point with R^2 values mostly above 0.9 (Table 5). Only Antarctic air masses during austral summer and autumn exhibit a lower correlation.

Air masses from the sectors eastern ocean and continental on the other hand show very low correlations with the averages observed at Cape Point indicating that these air masses differ significantly from the rest. On average, transport from these two regions make up 10% of the air masses at Cape Point (Table 1). Their prevalence varies mostly only by 1 to 2 percentage points from year to year with a peak of 10% continental air masses in 2011. However, we found that the prevalence of air masses from source and sink regions is not the driver of the inter-annual variability of Hg concentrations at Cape Point. (e.g. even with twice as much as average air masses from the sink region 2011 was no year with particularly low Hg concentrations) (Figs. 8, 9). Because of this and based on the comparison with measurements at Amsterdam Island (Slemr et al., 2020) we are confident that mercury concentrations observed at Cape Point are representative for the southern hemisphere background. Additionally, based on the presented work we are able to filter out the source and sink regions from the dataset for further analysis. Figure 10 depicts the whole GEM dataset with values from source and sink regions highlighted.

	Annual	Spring (SON)	Summer (DJF)	Autumn (MAM)	Winter (JJA)

Antarctic	0.89	0.95	**0.75**	**0.72**	0.96
South American	0.95	0.95	0.91	0.95	0.97
Continental	**0.39**	**0.54**	**0.05**	**0.59**	**0.33**
Eastern Ocean	0.81	0.77	**0.58**	**0.14**	0.84
Atlantic	0.98	0.97	0.90	0.94	0.99

Table 5: Correlation coefficient (R^2) of regional average concentrations with averages of all measurements at Cape Point. Values are based on monthly averages (N=30). Antarctic, Atlantic, and South American air masses exhibit a high correlation with the overall mean concentrations observed at Cape Point.

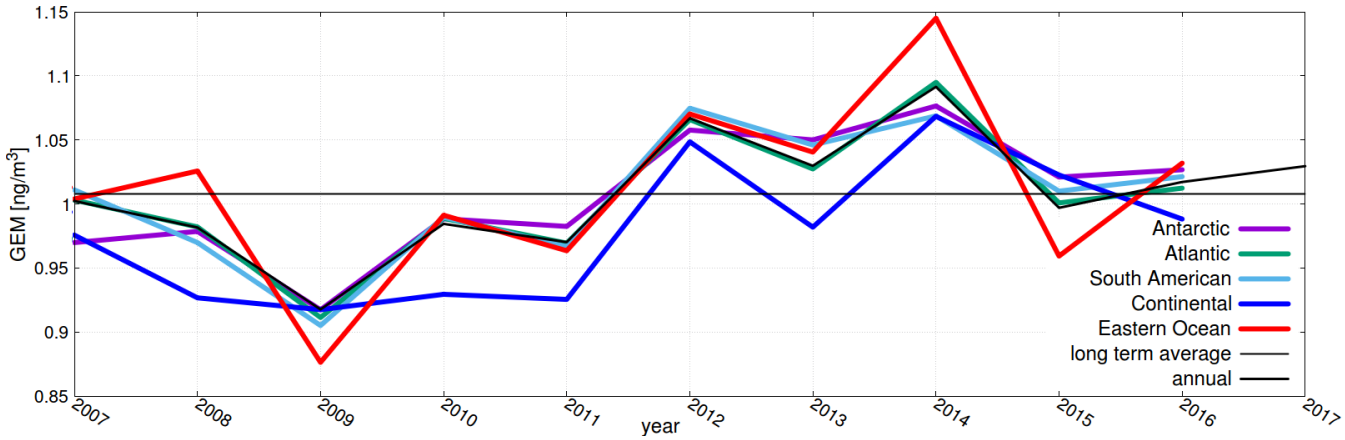

Figure 9: Annual average concentrations at Cape Point from 2007 to 2017 (black line) and regional averages (colored lines). It can be seen that the minimum in 2009 and the maximum in 2014 is present in all source regions.

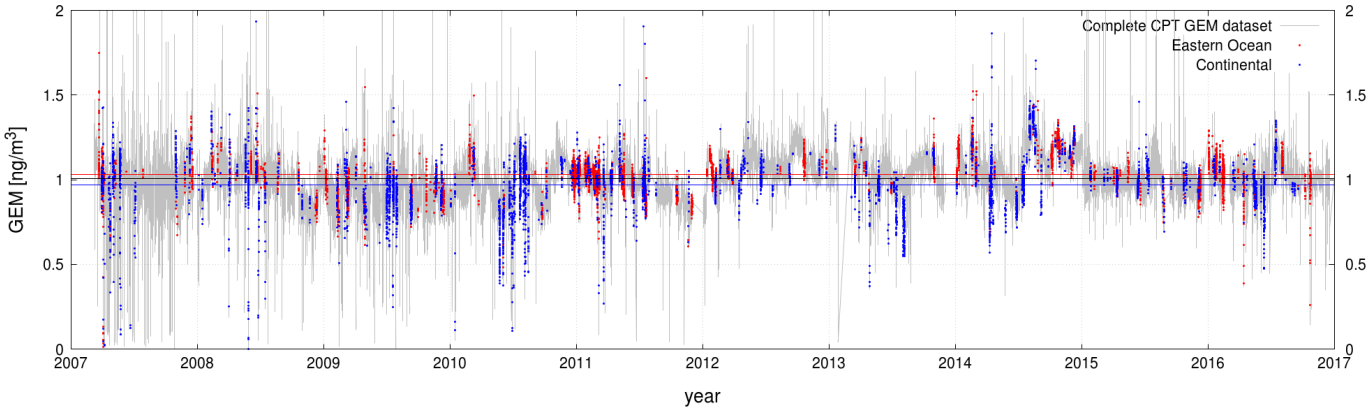

Fig. 10 Complete Cape Point dataset (grey) with observations originating from source (red) and sink (blue) regions superimposed. The colored x-axis parallel indicates the long-term average (black: complete dataset, red: source region, blue: sink region).

3.5 Inter-annual variability

The trend in GEM concentrations observed at Cape Point and the fact that it seemingly changed from increasing to stable between 2006 and 2017 is still unexplained (Slemr et al., 2020). Having shown that the observations at Cape Point are not dominated by regional processes the question arises which large-scale processes modulate the signal on annual and decadal time scales.

At this point, our null hypothesis is that mercury concentrations in the southern hemisphere were stable over the last decade but processes on global and hemispheric scales superimpose a (multi-)annual modulation on the signal. Based on our analysis so far, we can exclude changes in climatology as the cause for the inter-annual variability. Thus, in our opinion only global source processes remain as possible explanations for the observed anomaly. The identified processes are: marine emissions, emissions from biomass burning and artisanal small scale (ASGM) gold mining which are the major sources for mercury in the Southern Hemisphere.

Especially, the low mercury concentrations observed in 2009 and the high values observed in 2014 seem to be at least partially a large-scale phenomenon. A screening of international observation networks showed that also Mace Head – which is located in the Atlantic Ocean in the northern hemisphere – also has the lowest annual average mercury concentrations in 2009 and the highest in 2014 (GMOS, 2020; Weigelt et al., 2015). For the year 2009 the mercury emission inventory of Streets et al. (2019) postulates a sudden plummet in global gold mining activity. Comparing the annual anomaly from the ten-year average, gold mining activity are correlated with observed GEM concentrations (R=0.64). Similarly, we found a correlation with biomass burning in the Southern Hemisphere (mostly Africa) (R=0.75) (Jiang et al., 2017). We removed air masses from the identified source and sink regions from the data set and used a regression analysis to correct for changes in global gold mining and biomass burning emissions (Figure 11). The resulting signal becomes relatively flat with only two peaks remaining in 2012 and 2014.

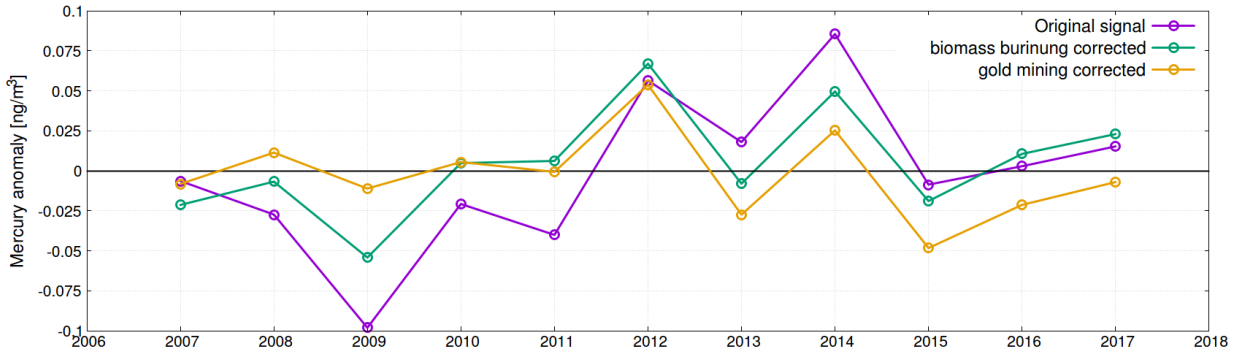

Fig. 11: Annual anomaly from ten-year average mercury concentrations. Original dataset at Cape Point (purple), corrected for biomass burning emissions (green) (Jiang et al., 2017) and additionally corrected for gold mining emissions (orange) (Streets et al., 2019).

4. Conclusions

Our goal was to improve the understanding of mercury cycling in the Southern Hemisphere. For this, we combined ten years of GEM observations at Cape Point, South Africa with hourly backward trajectories calculated with the Hybrid Single Particle Lagrangian Trajectory (HYSPLIT) model. Our findings are that:

(1) Overall the continent is a major sink region for mercury despite significant point sources, mostly linked to coal combustion.

(2) Mercury emissions from the warm Agulhas current to the south-east are a major source of elevated Hg concentration observed at Cape Point.

(3) Separating the ground-based observations into air parcels from different source regions showed that mercury behaves opposite to known pollutants of terrestrial origin implying the ocean as its major source.

(4) Mercury concentration in air masses from Antarctic, Atlantic, and south American origin were statistically almost indistinguishable. Thus, we interpret these observations as a good representation of the southern hemispheric background.

(5) We find that the trends in GEM concentrations postulated in the past are probably an artifact of single years with unusually high (2014) or low (2009) GEM concentrations (see accompanying paper: Slemr et al., 2020). We have shown that these exceptional years could be partly explained by changes in global emissions from biomass burning and gold mining, two major sources of mercury in the Southern Hemisphere.

(6) With the Ocean being the main source of mercury in the southern hemisphere it can be expected that an increased air-sea flux due to larger concentration gradients will compensate reductions in global atmospheric emissions due to the Minamata Convention. With this in mind we emphasize the need for more research on marine mercury dynamics and air-sea exchange of mercury.

References

Amos, H. M., D. J. Jacob, D. G. Streets, and E. M. Sunderland (2013), Legacy impacts of all-time anthropogenic emissions on the global mercury cycle, Global Biogeochem. Cycles, 27, 410–421, doi:10.1002/gbc.20040.

Baker, P.G.L., Brunke, E.-G., Slemr, F., Crouch, A. (2002), Atmospheric mercury measurements at Cape Point, South Africa. Atmos. Envron. 36 (14) 2459-2465.

Belelie, M.D., Piketh, S.J., Burger, R.P., Venter, A.D., Naidoo, M., 2018. Characterisation of ambient Total Gaseous Mercury concentrations over the South African Highveld. Atmospheric Pollut. Res. https://doi.org/10.1016/j.apr.2018.06.001

Brunke, E.-G., Labuschagne, C., Parker, B., Scheel, H.E., Whittlestone, S., 2004. Baseline air mass selection at Cape Point, South Africa: application of 222Rn and other filter criteria to CO2. Atmos. Environ. 38, 5693–5702. https://doi.org/10.1016/j.atmosenv.2004.04.024

Brunke, E.-G., Labuschagne, C., Ebinghaus, R., Kock, H. H., Slemr, F. (2010), Gaseous

elemental mercury depletion events observed at Cape Point during 2007-2008. Atmos. Chem. Phys., 10, 1121-1131, 2010.
Buishand, T.A., 1982. Some methods for testing the homogeneity of rainfall records. J. Hydrol. 58, 11–27. https://doi.org/10.1016/0022-1694(82)90066-X
Carslaw, D.C., and Ropkins, K.: *openair* – An R package for air quality analysis, Environ. Modelling Software, 27-28, 52-61, 2012.
Engström and Magnusson, 2009, https://www.atmos-chem-phys.net/9/8857/2009/acp-9-8857-2009.pdf
Fischer, H., Pozzer, A., Schmitt, T., Jöckel, P., Klippel, T., Taraborrelli, D., and Leleieveld, J.: Hydrogen peroxide in the marine boundary layer over the South Atlantic during the OOMPH cruise in March 2007, Atmos. Chem. Phys., 15, 6971-6980, 2015.
GMOS, Global Mercury Observation System, 2020. Available online: http://sdi.iia.cnr.it/geoint/publicpage/GMOS/gmos_monitor.zul
Gschwend, P.M., Macfarlane, J.. K., Newman, K.A., 1985. Volatile halogenated organic compounds released to seawater from temperate marine macroalgae. Science 227, 1033–1035.
Jiang, Z., Worden, J.R., Worden, H., Deeler, M., Jones, D.B.A., Arellano, A.F., and Henze, D.K.: A 15-year record of CO emissions constrained by MOPITT CO observations, Atmos. Chem. Phys., 17, 4565-4583, 2017.
Kaiser R. and Gottschalk G., (1972), Elementare Tests zur Beurteilung von Messdaten. Bibliographisches Institut.
Kalnay, E., Kanamitsu, M., Kistler, R., Collins, W., Deaven, D., Gandin, L., Iredell, M., Saha, S., White, G., Woollen, J., Zhu, Y., Chelliah, M., Ebisuzaki, W., Higgins, W., Janowiak, J., Mo, K.C., Ropelewski, C., Wang, J., Leetmaa, A., Reynolds, R., Jenne, R., and Joseph, D.: The NCEP/NCAR 40-year reanalysis project, Bull. Amer. Meteor. Soc., 77, 437-470, 1996.
Martin, L.G., Labuschagne, C., Brunke, E.-G., Weigelt, A., Ebinghaus, R., Slemr, F., 2017. Trend of atmospheric mercury concentrations at Cape Point for 1995–2004 and since 2007. Atmos. Chem. Phys., 17, 2393–2399.
Monks, P.S., Carpenter, L.J., Penkett, S.A., Ayers, G.P., Gillett, R.W., Galbally, I.E., and Meyer, C.P.: Fundamental ozone photochemistry in the remote marine boundary layer: the SOAPEX experiment, measurement and theory, Atmos. Environ., 32, 3647-3664, 1998.
NOAA Air Resources Laboratory (ARL), 2004, http://ready.arl.noaa.gov/gdas1.php, Tech. rep.
Slemr, F., Brunke, E.-G., Labuschagne, C., and Ebinghaus, R.: Total gaseous mercury concentrations at the Cape Point GAW station and their seasonality, Geophys. Res. Lett., 35, L11807,doi:10.1029/2008GL033741, 2008.
Slemr, F., Brunke, E.-G., Whittlestone, S., Zahorowski, W., Ebinghaus, R., Kock, H.H., and Labuschagne, C.: ^{222}Rn-calibrated mercury fluxes from terrestrial surface of southern Africa, Atmos. Chem. Phys., 13, 6421-6428, 2013.
Slemr, F., Weigelt, A., Ebinghaus, R., Bieser, J., Brenninkmeijer, C.A., Rauthe-Schöch, A., Hermann, M., Martinsson, B.G., van Velthoven, P., Bönisch, H., Neumeier, M., Zahn, A., Ziereis, H., 2018. Mercury distribution in the upper troposphere and lowermost stratosphere according to measurements by the IAGOS-CARIBIC observatory: 2014–2016. Atmos. Chem. Phys., 18, 12329-12343
Slemr, F., Martin, L., Labuschagne, C., Mokolo, T., Angot, H., Magand, O., Dommergue, A., Garat, P., Ramonet, M., Bieser, J. 2020. Atmospheric mercury in the southern hemisphere – Part 1: Trend and inter-annual variations of atmospheric mercury at Cape Point, South Africa, in 2007-2017, and on Amsterdam Island in 2012 – 2017. Atmos. Chem. Phys. https://doi.org/10.5194/acp-2020-70
Stein, A. F.; Draxler, R. R.; Rolph, G. D.; Stunder, B. J. B.; Cohen, M. D.; Ngan, F. NOAA's HYSPLIT Atmospheric Transport and Dispersion Modeling System. *Bull. Amer. Meteor.*

Soc. **2015**, *96* (12), 2059–2077.
Streets, D.G., Horowitz, H.M., Lu, Z., Levin, L., Thackray, C.P., and Sunderland, E.M.: Global and regional trends in mercury emissions and concentrations, 2010- 2015, Atmos. Environ., 201, 417-427, 2019.
UNEP: The Minamata Convention on Mercury, available at: http://www.mercuryconvention.org/Countries/tabid/3428/language/en-US/Default.aspx, (last access: June 2019), 2013.
Venter, A.D., Beukes, J.P., van Zyl, P.G., Brunke, E.-G., Labuschagne, C., Slemr, F., Ebinghaus, R., Kock, H., 2015. Statistical exploration of gaseous elemental mercury (GEM) measured at Cape Point from 2007 to 2011. Atmos Chem Phys 15, 10271–10280. https://doi.org/10.5194/acp-15-10271-2015
Weigelt, A., Ebinghaus, R., Manning, A.J., Derwent, R.G., Simmonds, P., Spain, T.G., Jennings, S.G., Slemr, F.: Analysis and interpretation of 18 years of mercury observations since 1996 at Mace Head, Ireland, Atmospheric Environment 100, 85-93, 2015.
Zahorowski, W., Chambers, S.D., and Henderson-Sellers, A.: Ground-based radon-222 observations and their application to atmospheric studies, J. Environ. Radioactivity, 76, 3-33, 2004.